PERGAMON

Atmospheric Environment 35 (2001) 3395–3404

ATMOSPHERIC ENVIRONMENT

www.elsevier.com/locate/atmosenv

Urban street-canyon flows with bottom heating

Jae-Jin Kim, Jong-Jin Baik*

Department of Environmental Science and Engineering, Kwangju Institute of Science and Technology, Kwangju 500-712, South Korea

Received 24 August 2000; received in revised form 15 January 2001; accepted 7 February 2001

Abstract

Urban street-canyon flows in the presence of street-bottom heating are investigated using a two-dimensional numerical model with a $k-\varepsilon$ turbulence closure scheme. The street aspect ratio (H/D, where H and D are the building height and the width between two buildings, respectively) varies from 0.6 to 3.6 (in 0.2 interval) and the initial potential temperature difference between the street-canyon bottom and the air ($\Delta\Theta$) ranges from 0 to 16 K (in 2 K interval). Five flow regimes are identified. Regime I is observed when the aspect ratio is very small but the bottom heating is very strong ($H/D = 0.6$ and $\Delta\Theta \geqslant 10$ K). In regime I, as the heating intensity increases, the thermally induced vortex expands but the mechanically induced vortex contracts. Regime II is mainly observed when the aspect ratio is relatively small or the bottom heating is weak. In regime II, the vortex intensity increases with increasing heating intensity. Regime III is observed when the bottom heating is relatively significant ($\Delta\Theta \geqslant 4$ K) and the aspect ratio lies in the range of 1.2–2. This regime differs from regime II in that the vortex induced by temperature gradient on the upwind side of the upper layer has meaningful intensity and size and the maximum horizontal velocity decreases with increasing heating intensity. When the bottom heating is relatively significant, regime IV is most commonly observed. This consists of two corotating vortices in the vertical within combined streamlines. Regime V exhibits two counterrotating vortices induced on both sides of the maximum temperature axis in the lower layer. The upper vortex is little influenced by the bottom heating. The numerical model result is shown to be reasonably in good agreement with the wind-tunnel data.

Keywords: Urban street-canyon flows; Flow regimes; Street aspect ratio; Bottom heating

1. Introduction

Urban flow and dispersion have been investigated actively during the past three decades, especially with an aim to evaluate proposals for improving air quality. In an urban street canyon which is a basic unit used to study a complex urban area, the flow pattern is determined by the ambient wind speed and direction, the geometry of building street, the sunshine duration, the albedo of building and road, and so on.

There are three kinds of flow patterns in street canyons; skimming flow, wake interference flow, and isolated roughness flow (Oke, 1988; Hunter et al., 1990/91, 1992). The skimming flow, which has been studied with a special interest in dispersion problem, exhibits either one vortex or multi-vortices restricted below the street-canyon roof level depending on the street aspect ratio. In this flow, the dispersion pattern strongly depends on the vortex number (Lee and Park, 1994; Baik and Kim, 1999). A field experiment in Chicago by DePaul and Sheih (1986) showed that the ambient wind should be relatively strong enough to maintain a vortex in a street canyon. The numerical result of Baik and Kim (1999) indicates that a critical ambient wind speed also exists in order to generate quasi-steady state two vortices. A wind tunnel experiment by Hoydysh and Dabberdt (1988) showed that the dispersion pattern around street canyons is strongly dependent upon the asymmetry of buildings but is less sensitive to the orientation of prevailing flow. Using a circulating water channel, Baik et al. (2000) found that the vortex number

*Corresponding author.
E-mail address: jjbaik@aromi.kjist.ac.kr (J.-J. Baik).

1352-2310/01/$ - see front matter
PII: S1352-2310(01)00135-2

as well as the vortex structure can vary as the ambient flow direction changes in a street canyon composed of buildings with different heights.

Besides the building/street geometry and meteorological conditions, thermal forcing such as building surface or street-canyon bottom heating is known to play an important role in determining flow pattern in street canyons (Sini et al., 1996; Kim and Baik, 1999). A temperature measurement in a street canyon with an aspect ratio of 1.06 and a sky view factor of 0.43 by Nakamura and Oke (1988) showed that the maximum temperature difference between the building surface and the air is as large as 12–14°C. Daily variation in temperature and its difference between the building surface (or street bottom) and the air in a street canyon are closely related to the sunshine duration, the sky view factor, and the albedo of building surface (or street bottom) (Sakakibara, 1996). Kim and Baik (1999) simulated urban street-canyon flows in the presence of upwind or downwind building wall heating or street-canyon bottom heating. They explained resultant flow fields in terms of mechanically and thermally induced circulations. In the upwind or downwind building wall heating cases, the vortex generation could be well explained for different aspect ratios. However, in the street-canyon bottom heating cases, flow patterns were shown to be relatively complicated and there remains something that needs to be investigated more systematically with different bottom-heating intensities and aspect ratios in order to further enhance our understanding of urban street-canyon flow and dispersion.

A main objective of this study is to characterize flow regimes according to various aspect ratios and heating intensities in a view of the vortex structure and intensity when the street-canyon bottom is heated. For this, a two-dimensional numerical model with a $k-\varepsilon$ turbulence closure scheme is employed.

2. Experimental setup

The numerical model used in this study is the same as that of Kim and Baik (1999). The model employs a two-dimensional, nonhydrostatic, nonrotating, and Boussinesq airflow system and the turbulent process is parameterized using a $k-\varepsilon$ turbulence closure scheme. The governing equations are solved on a staggered grid system using the finite volume method (Patankar, 1980). Fig. 1 shows the model domain configuration. In all numerical simulations, it is assumed that the street-canyon bottom is heated homogeneously. At the ground and building surfaces, the no-slip boundary condition is employed. To represent effectively the heat transfer between the street-canyon bottom and the air, a wall function is used. The domain sizes in the horizontal and vertical directions are 100 and 160 m, respectively. The grid interval is 2 m in both directions and the time interval is 0.1 s. The width between the upwind and downwind buildings is 40 m. An aspect ratio is defined as the ratio of the building height (H) to the street width (D). For a systematic investigation of flow regimes, 16 different aspect ratios are considered and for each aspect

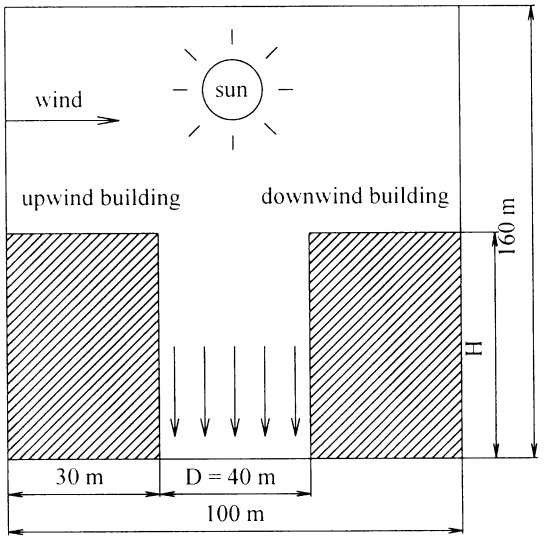

Fig. 1. The model domain configuration for this study.

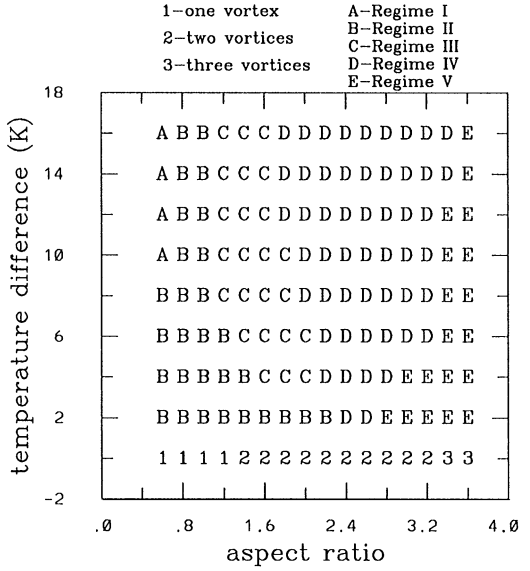

Fig. 2. Five flow regimes according to the aspect ratio and temperature difference.

ratio nine heating scenarios are examined ($\Delta\Theta = 0$, 2, 4, 6, 8, 10, 12, 14, 16 K). Here, $\Delta\Theta$ is the initial potential temperature difference between the street-canyon bottom and the air. During the time integration, the temperature at the street-canyon bottom is fixed. The aspect ratio ranges from 0.6 to 3.6 with an increment of 0.2. The initial air temperature is 293 K. The inflow wind profile at the left boundary has a power-law structure of $U_0 = 2.5(z/10)^{0.299}$, where U_0 is in m s^{-1} and z is in m. At the inflow boundary, the shear layer given by the profile is assumed to exist up to $z = 10$ m above the building roof level and above it the wind speed is assumed to be constant. For further details of numerical model and initial and boundary conditions, see Kim and Baik (1999).

3. Results and discussion

The numerical simulation data analyzed in this study are obtained at $t = 3600$ s, where all simulated urban street-canyon mean flows exhibit quasi-steady states. Fig. 2 shows flow regimes according to the aspect ratio and heating intensity (that is, the initial potential temperature difference between the street-canyon bottom and the air). Simulated street-canyon flows are classified into five regimes in a view of the vortex structure and intensity. Note that when there is no bottom heating, one vortex is formed in street canyons with aspect ratios of 0.6–1.2, two vortices are formed with aspect ratios of 1.4–3.2, and three vortices with aspect ratios of 3.4 and 3.6.

Regime I: This flow regime, which could not be identified in Kim and Baik's (1999) study because of relatively small temperature difference, occurs when the aspect ratio is very small but the heating intensity is relatively strong. In our simulations, regime I appears only when the aspect ratio is 0.6 and the temperature difference is greater than or equal to 10 K.

Fig. 3 shows the streamline and potential temperature fields when the aspect ratio is 0.6 and the temperature difference ($\Delta\Theta$) is 10 K. Two counterrotating vortices which are located horizontally in the street canyon are observed (Fig. 3a). When the aspect ratio is very small and the heating is very strong (regime I), the upward motion induced by buoyancy forcing is stronger than the horizontal motion of the reversed flow. As a result, the

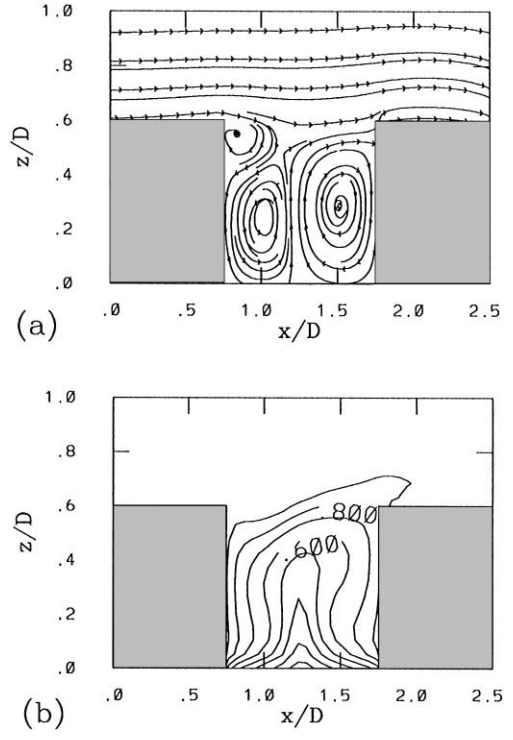

Fig. 3. (a) Streamline and (b) normalized potential temperature fields for an aspect ratio of 0.6 and a potential temperature difference of 10 K. The potential temperature is normalized by $(\Theta_{max} - \Theta(x, z))/(\Theta_{max} - \Theta_{min})$, where Θ_{max} and Θ_{min} are the maximum and minimum potential temperatures, respectively. The contour interval is 0.1. The horizontal and vertical axes in streamline and normalized potential temperature fields in this and other figures are normalized by the width between buildings (D).

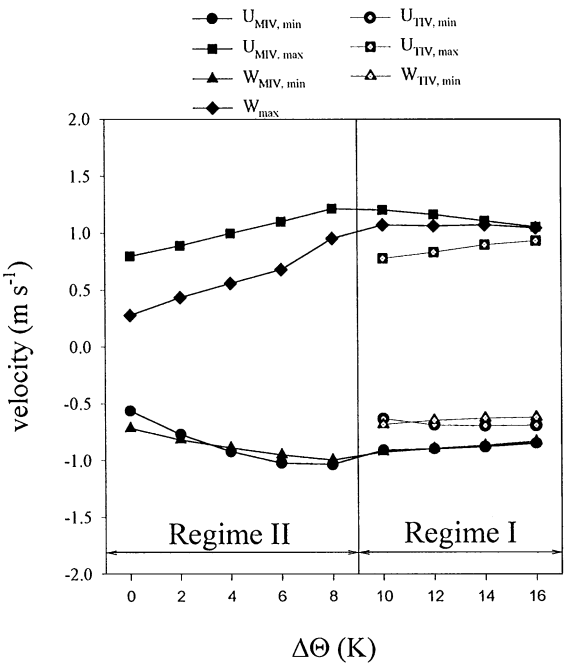

Fig. 4. Maximum and minimum horizontal and vertical velocities as a function of heating intensity. The aspect ratio is 0.6. The subscripts MIV, TIV, max, and min denote the mechanically induced vortex, thermally induced vortex, maximum, and minimum, respectively.

vortex is divided into two vortices, that is, a thermally induced vortex (TIV) on the upwind side and a mechanically induced vortex (MIV) on the downwind side and the maximum temperature axis is located near the center of the street canyon.

Fig. 4 shows the maximum and minimum horizontal and vertical velocities as a function of heating intensity when the aspect ratio is 0.6. In regime I, the magnitudes of all velocity components associated with MIV ($U_{\mathrm{MIV,max}}$, $U_{\mathrm{MIV,min}}$, W_{max}, and $W_{\mathrm{MIV,min}}$) decrease with increasing heating intensity. However, the magnitudes of the horizontal velocity components associated with TIV ($U_{\mathrm{TIV,max}}$, and $U_{\mathrm{TIV,min}}$) increase with increasing heating intensity in spite of a slight decrease in the magnitude of $W_{\mathrm{TIV,min}}$. Note that the maximum vertical velocity (W_{max}) occurs near the boundary between MIV and TIV. As the heating intensity ($\Delta\Theta$) increases, TIV expands but MIV contracts (not shown). This is a typical characteristic of regime I.

Regime II: This flow regime mainly appears when the aspect ratio is relatively small or the heating intensity is weak (Fig. 2). Fig. 5 shows the streamline fields with a potential temperature difference of 2 K in the cases of the aspect ratios of 1.2 and 1.8, together with the cases in which there is no bottom heating. In the cases of the aspect ratios of 1.2 and 1.8 without bottom heating (Figs. 5a and b, respectively), one vortex and two vortices are observed, respectively. When the temperature difference is 2 K, one vortex is generated in both cases (Figs. 5c and d). In the case of the aspect ratio at which one vortex is formed when there is no bottom heating, the maximum temperature axis is located near the upwind building because of its shift by the reversed flow. Therefore, the upward motion by buoyancy force is induced near the upwind building. This thermal upward motion makes the vortex stronger by reinforcing the mechanical upward motion near the upwind building. With an aspect ratio of 1.8, the bottom heating

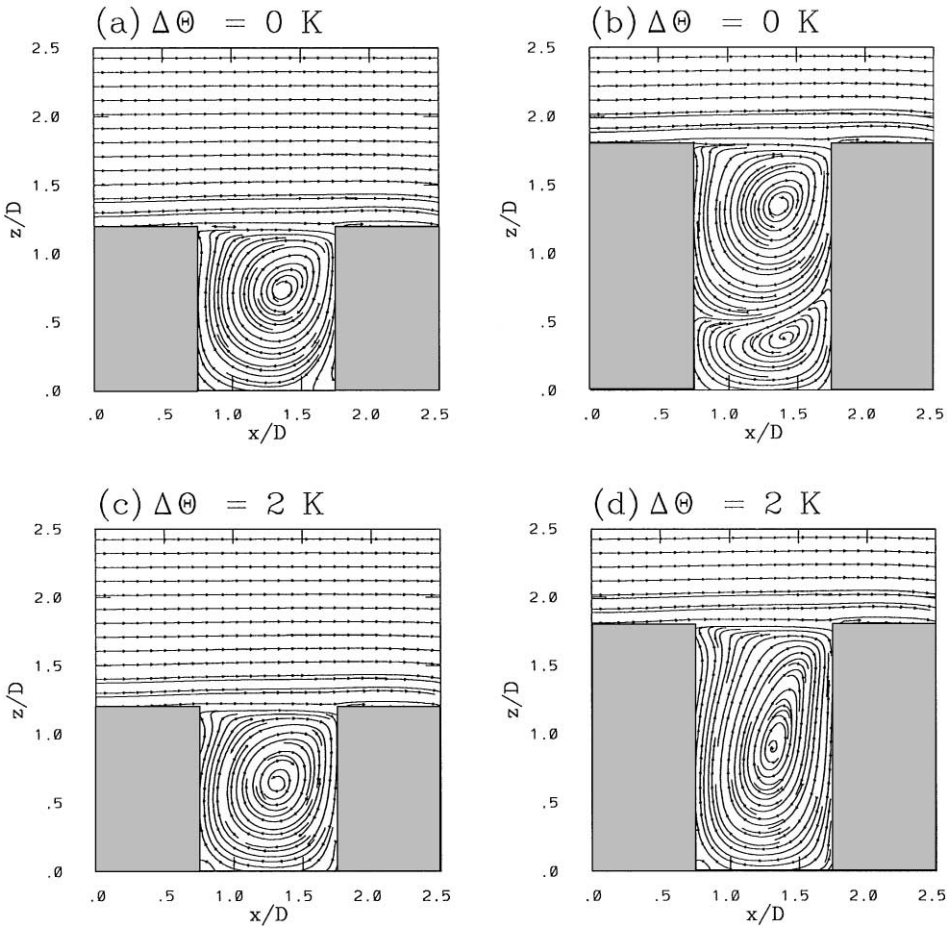

Fig. 5. The streamline fields for aspect ratios of 1.2 ((a) and (c)) and 1.8 ((b) and (d)) with no heating and a potential temperature difference of 2 K.

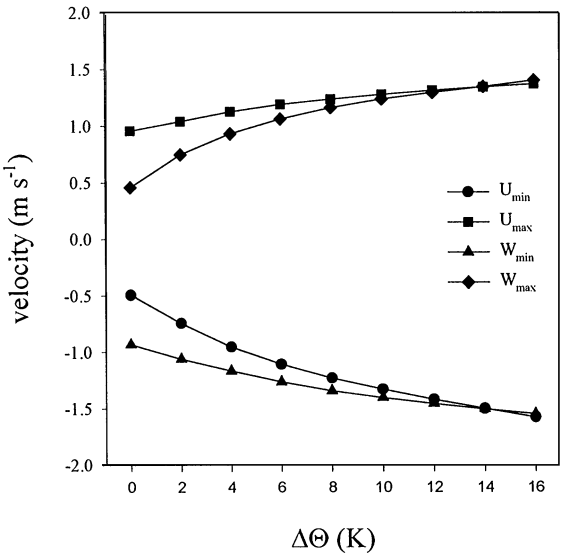

Fig. 6. Maximum and minimum horizontal and vertical velocities as a function of heating intensity. The aspect ratio is one. The subscripts max and min denote the maximum and minimum, respectively.

results in one reinforced vortex by removing the lower vortex (Figs. 5b and d). At the initial heating stage, the maximum temperature axis is located near the street-canyon center. The thermal upward motion around the maximum temperature axis divides the lower vortex into two. At the next stage, the clockwise rotating vortex on the downwind side of the lower layer begins to be merged into the upper vortex. Eventually, a single vortex forms. Moreover, the combined vortex becomes stronger and the vortex on the upwind side of the lower layer disappears. Hence, one reinforced vortex is formed and its intensity increases with increasing heating intensity.

Fig. 6 shows the maximum and minimum horizontal and vertical velocities as a function of heating intensity when the aspect ratio is one. The magnitudes of all velocity components increase with increasing heating intensity. This is because the bottom heating reinforces the intensity of MIV by inducing the upward motion around the maximum temperature axis which is shifted to the upwind side. In regime I, the bottom heating decreases the intensity of MIV. On the other hand, in regime II, the bottom heating increases the intensity of MIV. This is a typical characteristic of regime II. When the aspect ratio is 0.6 in regime II, the magnitudes of all velocity components increase as the heating intensity increases (Fig. 4).

Regime III: This flow regime mainly appears when the bottom heating is relatively significant ($\Delta\Theta \geqslant 4$ K) and the street canyon has aspect ratios in the range of 1.2–2 (Fig. 2). Regime III is similar to regime II in that one main vortex is formed (Figs. 7a and c). Although a small vortex is often observed near the upwind building in the upper layer in regime II, its size and intensity are negligible compared with those of the main vortex. However, in regime III, it is relatively large and intense. The temperature gradient (Figs. 7b and d) is responsible for the generation of the small vortex in the canyon. The vortex results from both the upward motion induced by positive buoyancy around the maximum temperature axis and the downward motion induced by negative buoyancy near the upwind building in the upper layer (see the horizontal line segment that crosses the center of the small vortex and the arrows in Fig. 7). The size and intensity of the small vortex increase as the aspect ratio and/or heating intensity increase.

Fig. 8 shows the maximum and minimum horizontal and vertical velocities as a function of heating intensity. The aspect ratio is 1.6. The magnitudes of $U_{\min}$, $W_{\max}$, and $W_{\min}$ increase with increasing heating intensity. This is also true in regime II (Fig. 6). Note that the maximum horizontal velocity ($U_{\max}$) decreases as the heating intensity increases. This is a typical characteristic of regime III and is considered to be related to the height of the vortex center. As the heating intensity increases, the vortex becomes stronger and the upper part of the vortex is extended as the vortex center is lowered (Figs. 7a and c). As a result, the maximum horizontal velocity in the upper layer decreases with increasing heating intensity in order to satisfy the mass conservation.

Regime IV: When the heating intensity is relatively significant, this flow regime was most commonly observed in the experiments. The process of the vortex formation is similar to that of regime III. The lower vortex in the no heating case is divided into two by the strong upward motion around the maximum temperature axis and then the upwind vortex is removed. The downwind vortex starts to be merged into the upper-layer vortex but this process remains incomplete. As a result, two clockwise rotating vortices in the vertical direction exist within the combined streamlines and a saddle point is present between two vortices (Fig. 9). The upper vortex is mechanically generated by the ambient wind. However, a main driving force of the lower vortex is the upward motion around the maximum temperature axis resulting from the street-canyon bottom heating. A small vortex in the upwind region is also observed in regime IV (Fig. 9). This small vortex in the mid-layer of the upwind region is generated by the temperature gradient and its size increases with heating intensity, as can be seen in Fig. 9.

Regime V: Fig. 10 shows the streamline fields in a street canyon with an aspect ratio of 3.6 when the temperature differences are 0, 4, 8, and 12 K. A notable characteristic of this regime is the existence of two

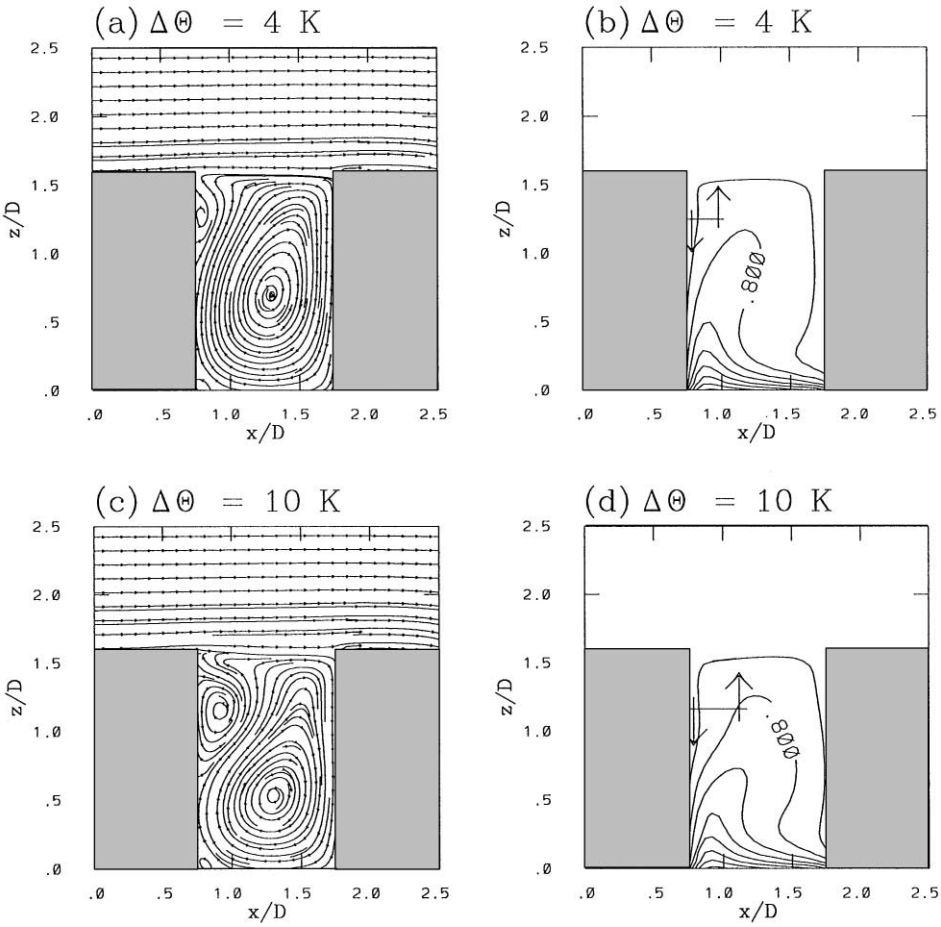

Fig. 7. Streamline ((a) and (c)) and normalized potential temperature fields ((b) and (d)) for an aspect ratio of 1.6 and potential temperature differences of 4 and 10 K. The horizontal line segment and arrows are drawn in (b) and (d) to explain the small vortex (see the text). The potential temperature is normalized by $(\Theta_{max} - \Theta(x, z))/(\Theta_{max} - \Theta_{min})$. The contour interval is 0.1.

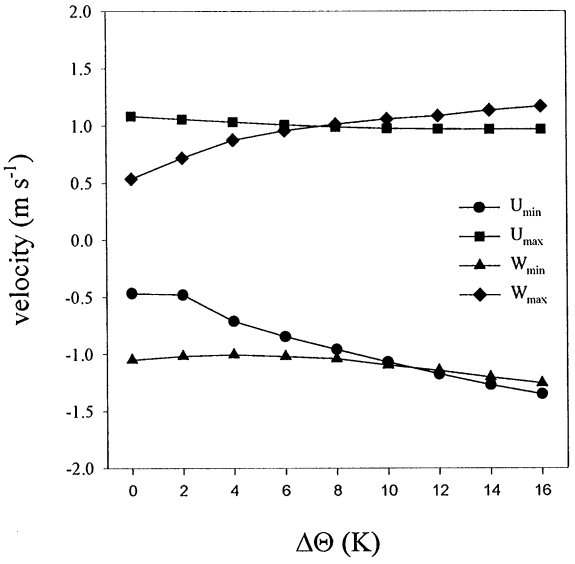

Fig. 8. The same as in Fig. 6 except for an aspect ratio of 1.6.

counterrotating vortices in the horizontal direction in the lower layer. In street canyons with relatively large aspect ratios, the thermally induced vortex in the upwind region of the lower layer is not extinguished and the upper vortex is little influenced by the bottom heating. However, in this flow regime, the magnitudes of the maximum horizontal and minimum vertical velocities observed in the upper vortex decrease slightly with increasing heating intensity (Fig. 11). When the heating intensity is relatively small, the minimum reversed flow (U_{min}) and the maximum upward motion (W_{max}) are observed in the upper vortex but as the heating intensity increases, U_{min} is observed in the downwind vortex in the lower layer and W_{max} around the maximum temperature axis. In the potential temperature fields (Fig. 12), the isotherm is almost symmetric around the maximum temperature axis. This is because the maximum temperature axis is little shifted by the weak horizontal motion at the initial heating stage and is located near the

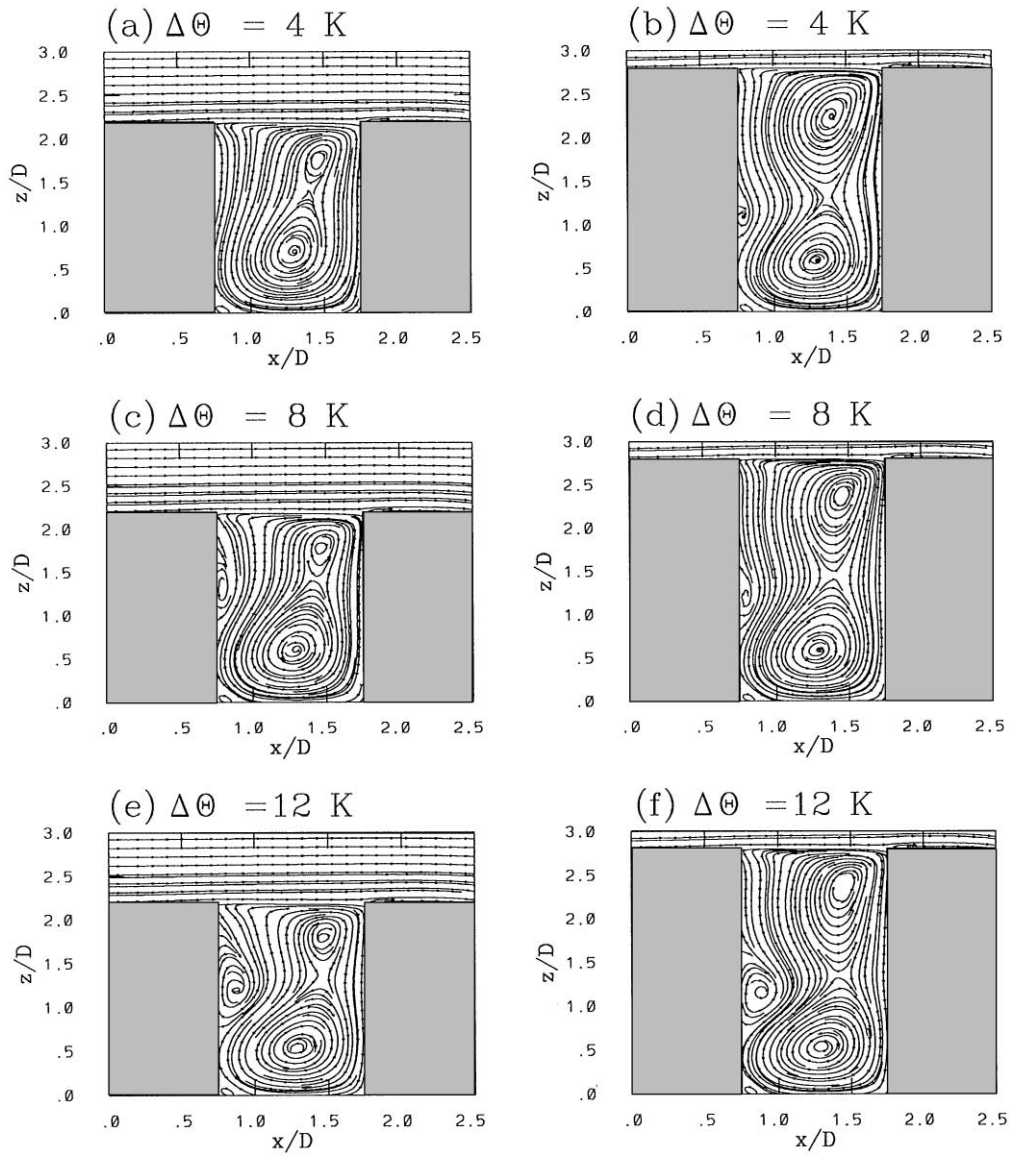

Fig. 9. Streamline fields for aspect ratios of 2.2 ((a), (c), and (e)) and 2.8 ((b), (d), and (f)) and potential temperature differences of 4, 8, and 12 K.

center of the street canyon. The upward motion around the maximum temperature axis induces two counter-rotating vortices in the lower layer. The two counter-rotating vortices becomes strengthened as the heating intensity increases.

4. Validation with the wind-tunnel data

For some validation, the model-simulation results with $H/D = 1$ and $\Delta\Theta = 2\,\mathrm{K}$ are compared with the wind-tunnel results with a bulk Richardson number, Rb, of -0.21 by Uehara et al. (2000). The bulk Richardson number is defined as

$$Rb = \frac{gH}{\Theta_0}(\Theta_a - \Theta_b)\frac{1}{U_a^2}, \tag{1}$$

where g, H, Θ, and U indicate gravitational acceleration, street-canyon height, potential temperature, and horizontal velocity, respectively. The subscripts, 0, a, and b indicate mean value within a street canyon, quantity at a roof-level, and quantity at the nearest grid

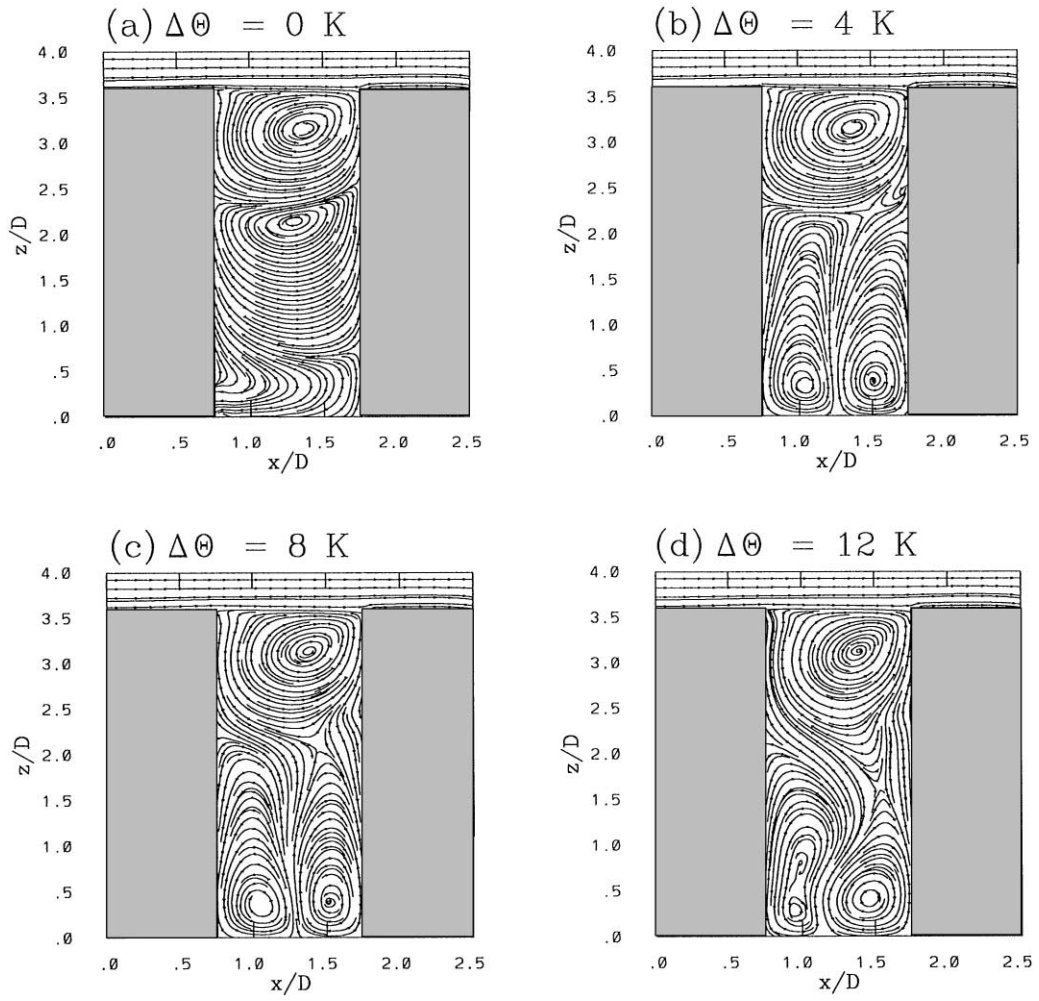

Fig. 10. Streamline fields for an aspect ratio of 3.6 and potential temperature differences of (a) 0 K, (b) 4 K, (c) 8 K, and (d) 12 K.

point from a street bottom, respectively. The computed *Rb* in the numerical simulation is −0.27. Fig. 13 shows the vertical profiles of the normalized potential temperature and horizontal velocity at the center of a street canyon with an aspect ratio of one. Except that the normalized potential temperature in the numerical simulation is lower than the wind-tunnel result in the lower layer ($z/H<0.2$), both profiles of the normalized potential temperature are very similar to each other. In the lower layer ($z/H<0.2$), the normalized horizontal velocity is weaker in the numerical simulation because of the application of no-slip boundary condition in the model. On the other hand, above a roof-level ($z/H>1.1$), the normalized horizontal velocity is stronger in the numerical simulation. This is related to the inflow boundary condition. In the numerical model simulation with an aspect ratio of 1, it is assumed that the profile of the horizontal velocity is constant above the height of 50 m at the inflow boundary. In spite of these differences, both profiles of the normalized horizontal velocity are overall similar to each other. From these results, the numerical model used in this study is considered to be appropriate for simulating urban street-canyon flows and identifying flow regimes in the presence of street-bottom heating.

5. Conclusion

A two-dimensional numerical model was employed to investigate urban street-canyon flows with street-bottom

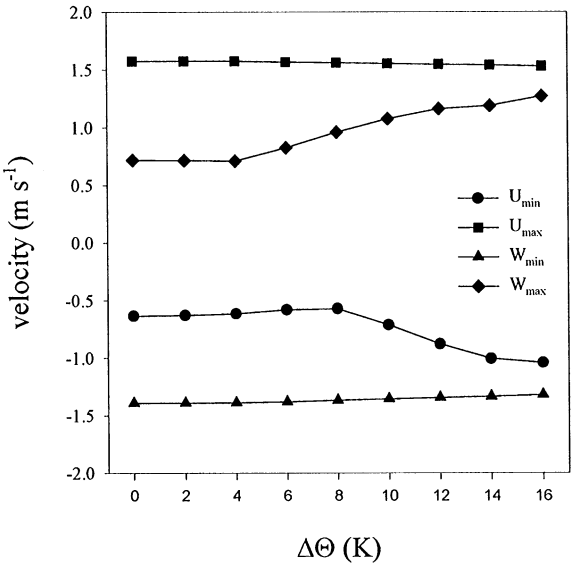

Fig. 11. The same as in Fig. 6 except for an aspect ratio of 3.6.

heating. Extensive simulations with various street aspect ratios and street-bottom heatings were performed to characterize flow regimes. Five flow regimes were identified: (I) flow with two counterrotating vortices, (II) flow with a thermally reinforced vortex, (III) flow with a thermally reinforced vortex and a thermally induced small vortex, (IV) flow with a vertically combined vortex, and (V) flow with two counterrotating vortices in the lower layer and a mechanically induced upper vortex. Results indicated that the thermal heating plays a significant role in determining flow fields within street canyons. The upward motion induced by buoyancy force can either strengthen or weaken vortex and modify vortex structure depending on the way that the thermally induced motion is combined with the mechanically induced motion.

In this study, pollutant dispersion in connection with street-canyon flows in the presence of street-bottom heating is not examined. Characterizing dispersion patterns when the street bottom is heated in the daytime is an important step in coping with air quality problem in cities. This needs to be investigated.

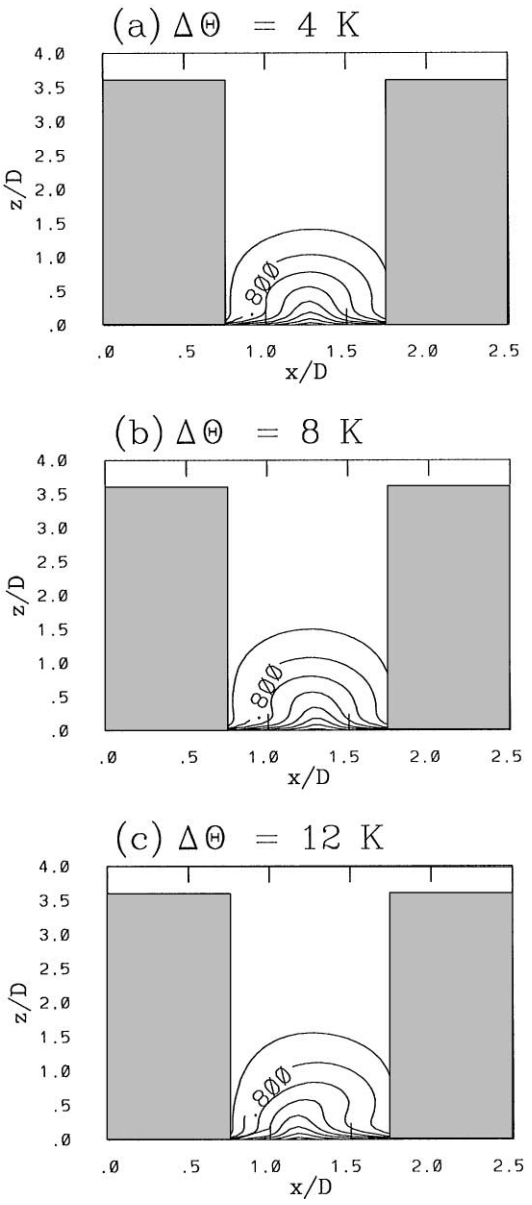

Fig. 12. Normalized potential temperature fields for an aspect ratio of 3.6 and potential temperature differences of (a) 4 K, (b) 8 K, and (c) 12 K. The potential temperature is normalized by $(\Theta_{max} - \Theta(x, z))/(\Theta_{max} - \Theta_{min})$. The contour interval is 0.1.

Acknowledgements

The authors are very grateful to two reviewers for providing valuable comments on this study. This research was supported by the Climate Environment System Research Center sponsored by the SRC Program of the Korea Science and Engineering Foundation. This research was also supported by the Brain Korea 21 Program.

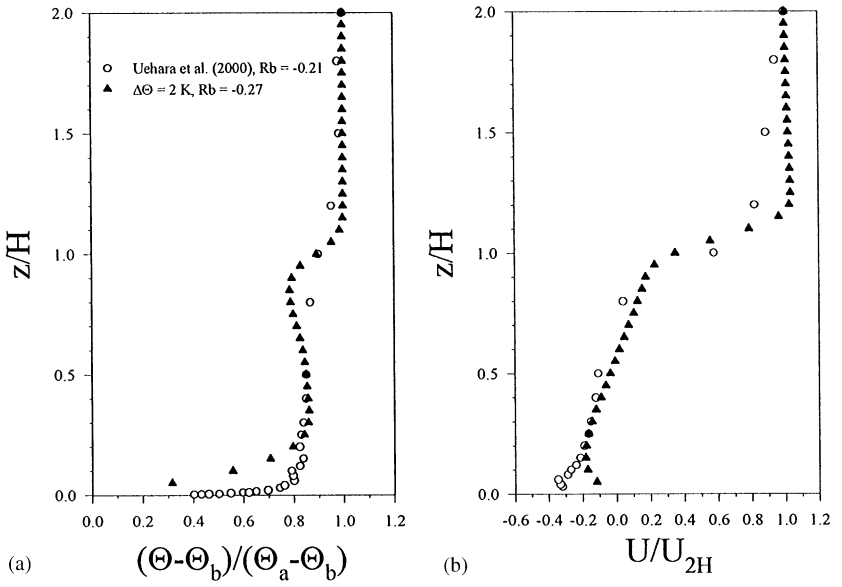

Fig. 13. Vertical profiles of normalized (a) potential temperature and (b) horizontal velocity at the center of a street canyon with an aspect ratio of one in the present numerical experiment and the wind-tunnel experiment of Uehara et al. (2000). H is the building height and U_{2H} is the horizontal velocity at the height of $z = 2H$.

References

Baik, J.-J., Kim, J.-J., 1999. A numerical study of flow and pollutant dispersion characteristics in urban street canyons. Journal of Applied Meteorology 38, 1576–1589.

Baik, J.-J., Park, R.-S., Chun, H.-Y., Kim, J.-J., 2000. A laboratory model of urban street-canyon flows. Journal of Applied Meteorology 39, 1592–1600.

DePaul, F.T., Sheih, C.M., 1986. Measurements of wind velocities in a street canyon. Atmospheric Environment 20, 455–459.

Hoydysh, W.G., Dabberdt, W.F., 1988. Kinematics and dispersion characteristics of flows in asymmetric street canyons. Atmospheric Environment 22, 2677–2689.

Hunter, L.J., Johnson, G.T., Watson, I.D., 1992. An investigation of three-dimensional characteristics of flow regimes within the urban canyon. Atmospheric Environment 26B, 425–432.

Hunter, L.J., Watson, I.D., Johnson, G.T., 1990/91. Modelling air flow regimes in urban canyons. Energy and Buildings 15–16, 315–324.

Kim, J.-J., Baik, J.-J., 1999. A numerical study of thermal effects on flow and pollutant dispersion in urban street canyons. Journal of Applied Meteorology 38, 1249–1261.

Lee, I.Y., Park, H.M., 1994. Parameterization of the pollutant transport and dispersion in urban street canyons. Atmospheric Environment 28, 2343–2349.

Nakamura, Y., Oke, T.R., 1988. Wind, temperature, and stability conditions in an east–west oriented urban canyon. Atmospheric Environment 22, 2691–2700.

Oke, T.R., 1988. Street design and urban canopy layer climate. Energy and Buildings 11, 103–113.

Patankar, S.V., 1980. Numerical Heat Transfer and Fluid Flow. McGraw-Hill, New York.

Sakakibara, Y., 1996. A numerical study of the effect of urban geometry upon the surface energy budget. Atmospheric Environment 30, 487–496.

Sini, J.-F., Anquetin, S., Mestayer, P.G., 1996. Pollutant dispersion and thermal effects in urban street canyons. Atmospheric Environment 30, 2659–2677.

Uehara, K., Murakami, S., Oikawa, S., Wakamatsu, S., 2000. Wind tunnel experiments on how thermal stratification affects flow in and above urban street canyons. Atmospheric Environment 34, 1553–1562.